40 years of ICRF operation on JET: challenges and achievements

Pierre Dumortier[1*], *Igor* Monakhov[2], *Philippe* Jacquet[2], *Frédéric* Durodié[1], *Ernesto* Lerche[1], *Robert* Lobel[2], *Marie-Line* Mayoral[2], *Craig* Noble[2], *Jason* Roberts[2], *Haroon* Sheikh[2], JET contributors[3], and the EUROfusion Tokamak Exploitation Team[4]

[1]LPP-ERM/KMS, B-1000 Brussels, Belgium, TEC partner
[2]UKAEA, Culham Centre for Fusion Energy, Abingdon, OX13 3DB, United Kingdom
[3]See author list of C.F. Maggi et al 2024 Nucl. Fusion 64 112012
[4]See author list of E. Joffrin et al., 2024 Nucl. Fusion 64 112019

Abstract. After 40 years of successful operation and multiple Deuterium-Tritium (D-T) campaigns, the Joint European Torus (JET) concluded its operations in December 2023. From the outset, Ion Cyclotron Range of Frequency (ICRF) heating was identified as a key auxiliary heating system, with the first ICRF system becoming operational in 1985. This system underwent significant development, culminating in a high-power (32 MW installed), wideband (23-57 MHz range), and highly versatile system. This contribution provides an overview of the JET RF system's evolution over its lifetime, highlighting selected operational challenges and technological achievements. It addresses the rationale behind the development and operation of the ICRF system, including the implementation and operation of load-resilient systems (3 dB hybrid coupler, External Conjugate-T, ILA), as well as the operational limits and system protection measures, such as the specific mode of operation for Ion Cyclotron Wall Conditioning (ICWC). The impact of transitioning from a carbon wall to the JET-ILW metal wall (tungsten divertor and beryllium first wall) on the system's operation and the challenges posed by D-T operations are also emphasized. Finally, key lessons learned from the technical challenges, constraints, and achievements of the JET experience are highlighted, with an eye towards the design and operation of ICRF systems in future machines.

1 The JET Project

The success of the tokamak [1] in the 1960s sparked a world-wide effort to further advance this type of fusion device by building larger devices with more ambitious goals. In Europe, this momentum led to discussions within the European Tokamak Advisory Group in 1971 about the development of a large-scale European tokamak. Later that year, the Joint European Torus (JET) working group was established. Following the recommendations of this group, a design team was formed at Culham Laboratory (UK) in 1973 to assess the feasibility of building a tokamak capable of bridging the gap between existing machines and a future fusion reactor. By 1975, the team completed the main design, which was fully detailed in their design proposal [2]. Culham was selected as the JET construction site in 1977 and on 25 June 1983, the first 50 ms hydrogen plasma pulse was successfully generated.

The primary objective of JET was to produce and study plasma in conditions and with dimensions that approach those needed for a fusion reactor [3, 4]. The four major areas of research included:

- Investigating plasma processes and determining scaling laws as parameters approach reactor conditions.
- Studying plasma-wall interactions and managing impurity influxes in those conditions.
- Demonstrating effective heating techniques to reach reactor-level temperatures (Ion Cyclotron Resonance Heating – ICRH, Neutral Beam Injection – NBI).
- Studying alpha-particle production, confinement and their role in plasma heating.

From the start, JET was designed with Deuterium-Tritium (D-T) operation in mind as well as confinement of alpha-particles. The design was chosen to be flexible, modular – composed of eight octants – and employing existing industrial techniques wherever feasible. Due to expected activation from D-T operation, remote handling was integrated into the project from the start. A pioneering design decision was the use of a D-shaped plasma configuration rather than the conventional circular shape. JET was an extraordinarily ambitious project, with design parameters exceeding all prior tokamak experiments. For instance, its plasma volume and heating power were each

* Corresponding author: pierre.dumortier@rma.ac.be

two orders of magnitude larger than any existing machine at the time.

All initial design goals were not only met but exceeded in various areas throughout JET's 40-year operational history. Over time, JET underwent several modifications, directly impacting its performance. The key events impacting RF operation were the X-point operation and subsequent H-mode operation for high performance plasmas, followed by the installation of the pumped divertor and finally the transition from a carbon wall (JET-C) to a metal wall (JET-ILW). These events, together with the tritium-based experiments are summarized in Table 1.

Table 1. JET timeline highlighting the major changes impacting the ICRF operation, the trace tritium campaign and the D-T Experimental campaigns (DTE).

Year	Event
25 June 1983	First Plasma
1986	X-point and first H-mode
1991	Preliminary Tritium Experiment
1992–1994	In-vessel coils and pumped divertor
1997	DTE1
2003	Trace Tritium Experiments
2009–2011	Be/W metal wall installation
2020–2021	100% Tritium and DTE2
2023	DTE3

The last JET pulse was performed on 18 December 2023. Excellent reviews of the technical and scientific achievements of the 40 years of JET operation can be found in [5, 6].

Throughout JET's lifetime, four generations of ICRF antennas were developed, each contributing to the system's evolution. The details of these advancements are covered in Sections 2 and 3.

2 The JET ICRF system

2.1 The genesis of ICRF heating on JET

In 1981, the decision was made to implement an ICRF system on JET, providing 15 MW of RF heating power to the plasma. This was based on a proposal from the Commissariat à l'Energie Atomique (CEA, France) in 1980, which outlined the physics principles and technical specifications required for an ICRF heating system [7]. Given that only half of the generated power would couple into the plasma, the initial plan was to install an ICRF plant capable of generating 30 MW of RF power [8]. This ambitious goal demanded unprecedented levels of power coupling – specifically, 1.5 MW per antenna for 10 s, equating to 15 MJ, a significant leap from the 0.1 MJ achieved in previous machines like TFR [9]. For the ICRF system, the main challenges to address were generating the required RF power, matching the RF system to the antenna and plasma load, optimizing the coupling of the power to the plasma and mitigating impurity production, a common issue in RF system operation.

The design philosophy centred around the use of proven technologies, rigorous antennas and system components testing (low and high voltage/current tests), and ensuring compatibility with D-T operation (activation, remote handling). The requirement of heating various ion species (hydrogen, deuterium, helium-3 and tritium) across different plasma conditions and magnetic fields led to the design of a highly flexible and versatile high power RF system, covering a broad frequency range (23-57MHz).

2.2 The JET ICRF plant and matching system

Initially, ten antennas and twenty 1.5 MW amplifiers were planned, but ultimately eight antennas and sixteen amplifiers were installed. These amplifiers, developed by Herfurth GmbH, were based on the TEXTOR amplifier design [10]. They were later upgraded to 2 MW in 1989, culminating in 32 MW of installed ICRF power [11]. They cover a broad operating frequency range: 23-57 MHz (except the inaccessible 39-41 MHz band) divided in eight bands of 4 MHz. They were moreover designed to be broad-band and allow 'instantaneous' frequency shifts within ±2 MHz of the tuned setting, which was a unique feature at these power levels and frequencies [8].

The power was transferred from the amplifiers to the antennas by 84 m long 30 Ω transmission lines, specially designed by Spinner GmbH for JET. These lines are 3 bar air pressurized and rated for 50 kV. As the antenna characteristic impedance of the first design was close to 25 Ω, a characteristic impedance of 30 Ω was chosen for the transmission lines to reduce mismatch [8, 12]. This characteristic impedance is also optimal for power handling. The matching was realized via tuning stubs at the generator end and frequency variation (≤100 kHz) to vary the long lines' electrical length. Pre-matching stubs could be installed close to the antenna and were used in certain conditions to reduce the voltage, current and losses on the long transmission lines [13, 14].

2.3 The A0 antennas

The antenna design phase, led by CEA (Fontenay-aux-Roses, France), drew from insights gained from smaller machines such as Erasmus [15], PLT [16], and TFR [9]. Several designs were considered (see Fig. 1), ultimately leading to the selection of a strap enclosed within a box with side walls and a Faraday screen [7]. To enhance coupling, the antennas were positioned as close to the plasma as possible, giving rise to the antenna-limiter concept – where the strap is enclosed within a box, shielded by a private limiter [12]. To reduce the RF-induced impurity level, the Faraday screen bars were tilted by 15° to align to the tokamak magnetic field and

the side protection limiters were composed of carbon, a low-Z material. Two types of interchangeable central conductors were implemented to test different shapes of radiated wave spectra. Dipole and quadrupole phasings were explored, alongside the – usual at the time – monopole phasing. The use of these alternative phasings was expected to decrease the impurity production, at the cost of reduced coupling [17, 18].

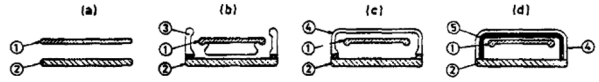

Fig. 1. Different considered strap designs: (a) without lateral part of the Faraday screen, (b) without Faraday screen in front of the plasma, (c) with a full Faraday screen and (d) with an alumina protection between the strap and the Faraday screen [7].

A picture of the resulting A0 prototype antennas is shown on Fig. 2. The antennas were mounted using the existing 150 mm diameter limiter guide tubes as feeding lines. One of the main aims of the A0 antennas was to give design and operational experience for optimising further antennas. These antennas were designed for short pulse operation and were consequently not actively cooled. The prototype antenna as well as the vacuum feedthroughs, which corona rings design was deemed critical, were tested up to 45 kV and 1.5 kA on a dedicated test-bed at Fontenay-aux-Roses [18]. The main difficulty encountered was the extent of the multipactor range, which could be reduced by silver coating the conductors. An exhaustive overview of the A0 design and tests is given in [19].

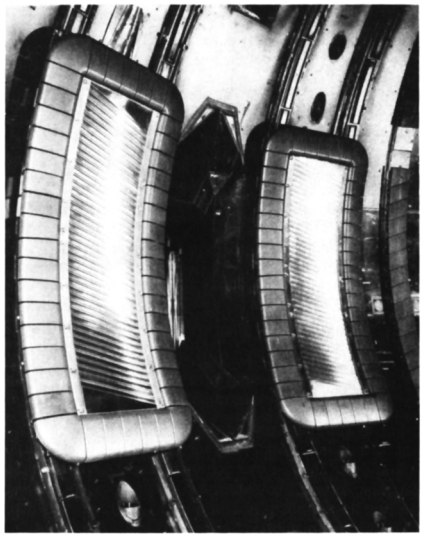

Fig. 2. Two A0 prototype antennas mounted on JET [19].

The two first A0 antennas were installed in 1984. The first supported monopole operation (out-of-phase feed) or dipole operation (in-phase feed), while the second supported dipole operation (in-phase feed) or quadrupole operation (out-of-phase feed) [13]. The first results of ICRF helium-3 (^{3}He) and hydrogen (H) minority heating in deuterium (D) with up to 2 MW coupled RF power have been reported in 1985 [3, 4]. A third unit has been installed in 1985 and 6 MW were coupled without issue by 3 antennas by the end of 1985 [20]. By 1987, up to 17 MW has been coupled to limiter plasmas. It was also observed that the impurity levels decreased with the dipole operation [21-23]. In 1987, the initial A0 antennas were replaced by eight actively cooled A1 antennas.

2.4 The A1 antennas

Eight so-called A1 antennas were installed in 1987, based on the A0 design and operational experience [24]. The aim was to deliver 12 MW of coupled power for 20 s. Eight generator units of 3 MW were installed by July 1987. The A1 antennas featured water-cooled nickel (Ni) Faraday screen bars and frame, with bars tilted to align with the tokamak magnetic field lines. The inner Vacuum Transmission Lines (VTLs) were cooled via forced gas flow. Two conical ceramics vacuum windows featuring advanced corona rings were mounted. Dipole ($k_{//}$=7 m^{-1}) and monopole ($k_{//}$=0 m^{-1}) operation were foreseen as well as the possibility to operate the current drive phasing (see Fig. 3). The coupling was improved so that the A1 dipole phasing operation would couple better than the A0 quadrupole operation. Again, all components of the antenna were extensively tested, up to 50 kV for 20 s on JET's dedicated test-bed. All components were silver plated (except the screen). An automatic matching system based on adjustable stubs, line stretchers and frequency shift was implemented, significantly simplifying operation [25, 26].

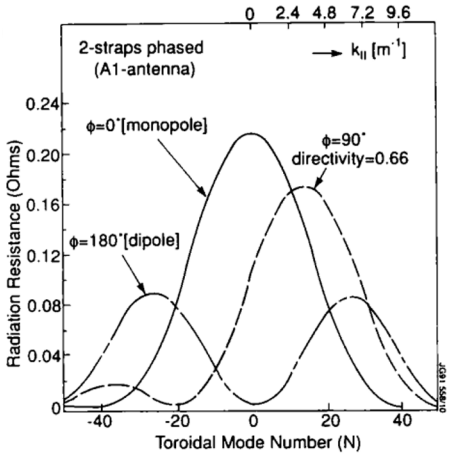

Fig. 3. Computed radiated power spectra at 0° (monopole), 180° (dipole) and 90° (current drive) for the A1 antenna [24].

Progress in the understanding of the mechanisms of RF induced impurity production and the role of the RF sheaths led to a new Faraday screen design, installed in 1989 [27, 28]. The nickel (Ni) Faraday screen was replaced by a beryllium (Be) Faraday screen, also with tilted bars. Beryllium's low atomic number (Z) and self-sputtering coefficient lower than unity made it a candidate of choice to reduce the impurity release. Furthermore, the improved conductivity of Be over Ni, together with the design of a more open screen, reduced the losses by an order of magnitude and allowed the Faraday screen bars to be cooled by conduction along the screen bars through their flexible end mountings rather than water cooled, greatly simplifying its design. The impurity release was further reduced by lowering the density at the Faraday screen using side limiters, the operation in dipole and the

use of machine conditioning techniques such as carbonisation and Be evaporation.

The A1 antennas achieved a wide range of results on JET, such as coupling a record 22 MW ICRF power to the plasma into a limiter L-mode plasma (H minority heating in D) [29], coupling 200 MJ into a single discharge, operating long pulses up to 60 s, producing RF-only H-mode and current drive operation. The operation on plasma was reliable up to 30 kV (corresponding to electric fields of about 2.2 kV/mm parallel to the magnetic field), beyond which arcing at the innermost conical ceramic supports of the VTLs imposed a voltage limit. Severe damage was observed at this location on two lines, which prompted for improved arc protection. A constant coupling resistance real time control was also developed for H-mode operation by feedback of the plasma position.

3 The installation of the pumped divertor

3.1 The A2 antennas

The installation of a pumped divertor on JET in 1992 significantly impacted the ICRF system. The two main consequences for the ICRF were the increased distance between the plasma and the wall, which would dramatically reduce the coupling of the installed A1 antennas to unacceptable levels, and the change in shape of the plasma, which became more top-down asymmetrical.

Moreover, the transition to H-mode operation, which became increasingly dominant following the installation of the pumped divertor, led to a further reduction in ICRH coupling, attributable to the distinct scrape-off layer properties between L- and H-modes. In particular, the steeper edge density gradients characteristic of H-mode in the region between the separatrix and the cut-off layer result in an increased refractive index mismatch, which consequently reduces the coupling [30-32].

Furthermore, the divertor plasma geometry introduced the need to avoid obstructing the tangential neutral beams. Half of the toroidal positions of the A1 antennas could not be re-used for the A2s. This entailed rebuilding half of the RF transmission lines in the basement and the torus hall.

Four new so-called A2 antennas were consequently designed [24], incorporating the return on experience from the A1 design and operation. The available space constraints allowed for a significant increase in antenna size. These antennas were 1.5 times wider and twice as deep as their predecessors, improving the expected coupling resistance by a factor 1.5 to 2. One A2 antenna was composed of 4 straps separated by a central septum to reduce the mutual coupling and ease the matching. The septum and sidewalls were slotted to minimise the spectrum degradation by the return currents. Additionally, the innermost conical ceramic VTL supports present in the A1 antennas, and which were limiting the operation in voltage, were eliminated, allowing for a more open VTL design and removing the need for private pumping of the VTL. An extra straight ceramic was subsequently added at the rear of the Antenna Pressurised Transmission Line (APTL) to counteract the radial loads on the A2 antenna straps resulting from the APTL air pressure acting over the area of the inner VTL bellows adjacent to the Double Conical Feedthrough (DCF).

Positioning the antennas deeper within the torus introduced concerns about disruption forces, prompting the adoption of a lightweight antenna box made from corrugated sheets, which minimized loop currents. Faraday screen bars were fitted with 0.1 Ω resistors to mitigate disruption forces. The high temperatures resulting from the thin sheet structure required nickel-coated housing and straps, while the VTL components were silver-coated for optimal conductivity. The Faraday screen bars were tilted between 13 and 18 degrees to match variations in the magnetic field along the antenna's height. The new poloidal limiters provided additional protection. The four-strap configuration produced a narrower wave spectrum than A1 antennas, enabling operation in various phasing modes, including current drive (see Fig. 4). These antennas were inertially cooled via radiation rather than active water cooling.

The A2 antennas were rigorously tested up to 42 kV - 20 s on a dedicated test-bed, although practical operation on plasma was typically limited to 30 kV. Penning gauges were employed to avoid operation with high pressure in the VTL and monitor the DCF interspace.

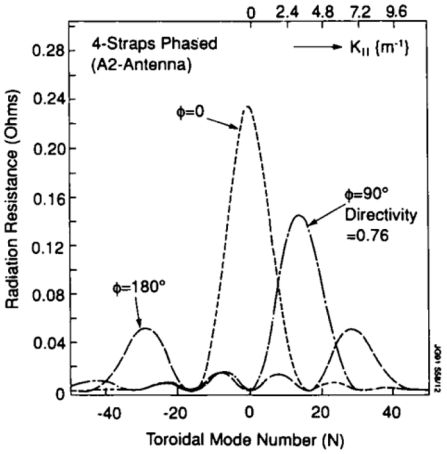

Fig. 4. Computed radiated power spectra at 0° (monopole), 180° (dipole) and 90° (current drive) for the A2 antenna [24].

The control system was upgraded to optimize arc detection, phase control, and power handling, ensuring reliable operation and preparing for long-pulse scenarios. Additionally, due to mutual coupling between strap pairs, two generators powering each half of an A2 antenna were linked. In 1996, a real-time monitoring and control system, known as the RF Local Manager (RFLM), was introduced.

Despite the careful design process, initial operation of the A2 antennas revealed some challenges [33]. Arcing to adjacent limiters was observed due to slotted sidewalls, and impedance mismatches in the cross-over feeds resulted in poor coupling of the two central straps, preventing monopole and phased array operation. These issues led to the removal of all A2 antennas during the 1995 shutdown to implement corrective measures. Modifications included adding high-capacitance plates to the cross-over feeds, installing flux excluders to reduce voltage differentials near limiters, and incorporating resistive flexible connectors at the top and bottom to

electrically integrate the antenna housing with horizontal rails. Following these refinements, the A2 antennas resumed operation without major issues and remained in service until the final shutdown of JET, marking an impressive 28-year lifespan.

3.2 Implementation of load-resilient schemes

The installation of the pumped divertor also brought new challenges related to load resilience. H-mode operation [34], which became dominant after the upgrade, was characterized by Edge Localized Modes (ELMs), resulting in rapid (<1ms) and complex – mostly resistive – load changes. Using the conventional matching scheme (see Fig. 5a), the RF amplifiers were systematically tripped during ELM events (associated with mismatch and high reflection), significantly limiting the ability to couple ICRF power to H-mode plasmas.

To ensure that RF sources remain properly matched despite these fast load transients, various matching systems have been developed, implemented, and tested over the years at JET [35-40].

3.2.1 The Sliding Impedance matching system (SLIMP)

Building on earlier capacitive stub pre-matching work, the SLIMP system was introduced in 1998 [39]. This system consisted of a high-impedance 105 Ω adjustable section positioned between two one-meter 24 Ω adjustable sleeves in each transmission line, located 18.5 m from the antenna. It was designed to provide broadband matching at 28, 36, 44, and 52 MHz. By adjusting the stub, trombone, and SLIMP positions, load variations were converted into phase shifts in the reflection coefficient, allowing the generator Voltage Standing Wave Ratio (VSWR) to remain low through frequency tuning and a fast frequency feedback system. However, due to its sensitivity to the electrical distance between the SLIMP starting point and the antenna short circuit, combined with complex set-up requirements, further development was discontinued.

3.2.2 The 3 dB hybrid coupler system

Installed between 2004 and 2005, the 3 dB hybrid coupler system (see Fig. 5b) was designed to feed both JET antenna arrays A and B [35]. This system operates by redirecting reflected power – caused by fast load transients such as those from ELMs – into a dummy load, ensuring steady conditions for RF generators during symmetric load transients. Experimentally validated on ASDEX-Upgrade, this technique is now a primary option for ITER. Although a small fraction of generated power is lost to the dummy loads during such events, significantly more power can be effectively delivered to the plasma, thanks to the avoidance of amplifier trips.

3.2.3 The External Conjugate-T (ECT)

The conjugate-T system connects pairs of straps to a T-junction, with impedance transformation elements added in each branch to create complex conjugate admittances to eliminate the susceptance at the T-junction and realize a target impedance Z_{CT} generally between 3 Ω and 6 Ω, which remains stable during rapid load changes. A second matching stage – including stub and trombone tuners – then transforms Z_{CT} to Z_0 (where Z_0 = 30 Ω at JET). Z_{CT} can have a small reactive part to equalize the voltages in case of asymmetries in the two branches of the conjugate-T.

The ECT (see Fig. 5c) was installed in 2007 on antenna arrays C and D, following a successful proof-of-principle demonstration on half of array C [38]. This system uses trombones in the transmission lines connecting the T-junction to the antenna straps to adjust impedance.

3.2.4 The ITER-Like Antenna (ILA) system

A new antenna, called ILA, was installed in 2007 (see Section 3.3). Whereas the ECT features a conjugate-T system with the matching components outside the vacuum vessel, the ILA system is based on the same principle but with the matching components, adjustable vacuum capacitors in this case, located inside the vacuum vessel (see Fig. 5d).

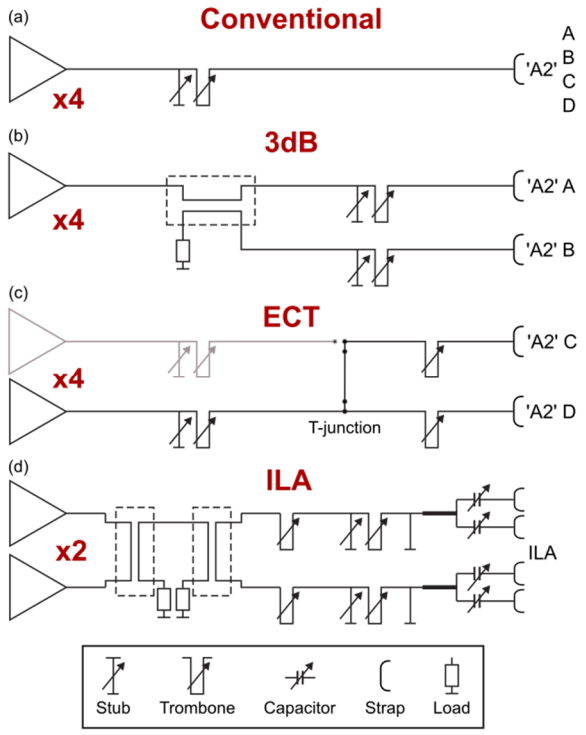

Fig. 5. Schematic of the different ICRF antenna and matching systems: (a) conventional matching system (b-d) ELM-resilient matching systems.

3.3 Towards high power density: the ILA

In view of reactor with limited wall space availability, it was decided to build a high power density antenna. The antenna was initially called JET-EP before being renamed ITER-Like Antenna or ILA. The ILA (see Fig. 6) [40-45] is a compact ion cyclotron port plug antenna composed of four Resonant Double Loops (RDLs) arranged in a 2 toroidal by 2 poloidal array. Each RDL consists of two poloidally adjacent short low-inductance straps fed through in-vessel matching vacuum capacitors from a common VTL. The matching is complemented by a quarter wave-length transformer (at 42.5MHz) and a

second matching stage consisting of a stub and a line stretcher (Fig. 5d). Two toroidally adjacent RDLs are powered through a 3 dB combiner-splitter arrangement linked to two 2 MW amplifiers. Internal matching, coupled with a second matching stage close to the antenna, effectively reduced power losses in the long transmission lines.

Although the ITER baseline has evolved over time – no longer incorporating internal matching components nor relying on Conjugate-T operation – several features of the ILA nevertheless remain relevant for ITER. These include the operation and control of tightly packed, high-power-density antenna arrays, validation of RF modelling and coupling predictions, ELM-resilient performance, high-voltage operation (>40 kV) and improved arc detection.

Up to 4.2 MW of power was coupled with the ILA into ELMy H-mode plasmas, corresponding to a power density exceeding three times that of the A2 antennas (3.8 MW/m² vs 1.2 MW/m², based on the antenna surface area definition proposed in [32]). Despite this increased power density, nickel impurity levels remained comparable to those observed with the A2s in JET-C [46, 47], and tungsten concentrations were lower than those observed with the A2s in JET-ILW [48].

A High Power Prototype of one quarter of the antenna was realized to validate the design [49] and the antenna was tested up to specifications on a dedicated test-bed at JET, where the voltage probes were also calibrated [50] and low power matching tests performed.

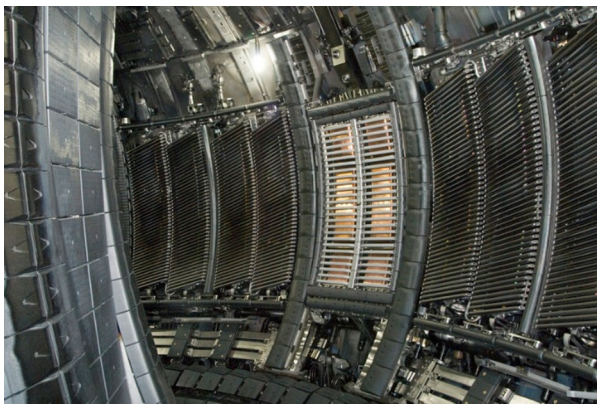

Fig. 6. Front view of the ILA antenna in between two A2 antennas in the JET vacuum vessel [43].

3.3.1 Full array control of the ILA

A major challenge was the full array control of a close-packed array like the ILA with large cross-talk [51, 52].

The first matching stage involves tuning the eight in-vessel capacitors to achieve the target complex conjugate-T point impedances ($Z_{T,req}$) for each of the four RDLs. For each RDL, the complex conjugate-T point impedance (Z_T) is derived using forward and reflected voltage data from the APTL directional coupler, together with a numerical RF circuit model.

Because of the strap asymmetry within individual RDLs, the ILA's load tolerance is inherently limited. This can be mitigated through a second stage offset matching process. The Second Stage Matching (SSM) system adjusts the lengths of four SSM stubs and four SSM trombones to reduce the peak excursions of the Main Transmission Line (MTL) Voltage Standing Wave Ratio (VSWR) observed during ELM events in ELMy plasma, rather than during inter-ELM intervals. A novel method was developed to implement this offset match: reflection coefficients in the MTL were recorded every 2 µs in both amplitude and phase, and mapped onto a polar diagram over a selected time window. The stubs and trombones were then adjusted more slowly to centre the system's response within the polar map of MTL reflection coefficients [53].

Given the ILA's reliance on the conjugate-T matching principle, another strategy to enhance load resilience is to operate at a lower real part of the T-point impedance, $Re(Z_T)$. Figure 7 illustrates improved load tolerance when $Re(Z_T)$ is reduced from 6 Ω to 3 Ω.

Antenna array phasing is fine-tuned by controlling the voltage probe signal phases of the four inner straps. Toroidal phase between adjacent RDLs is regulated by adjusting the four MTL trombones positioned at the outputs of the 3 dB combiner-splitters. Poloidal phase – defined as the phase shift between poloidally adjacent RDLs – is set relative to a separate phase reference and adjusted via the output phases of the four amplifiers. Since each 3 dB combiner-splitter is powered by two amplifiers, their output phases are inherently linked.

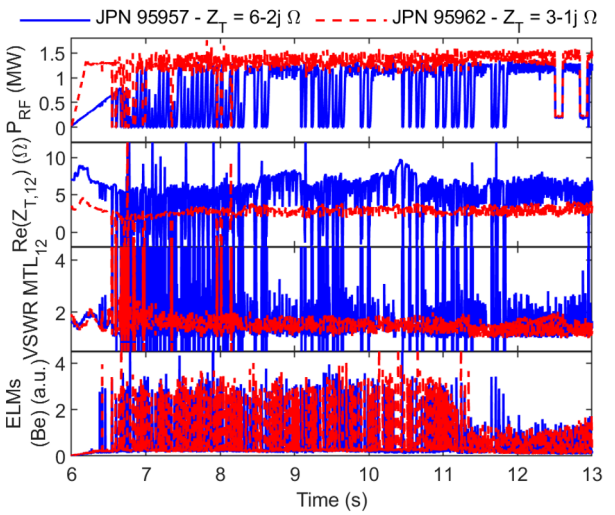

Fig. 7. Example of improved load-resilience with operation at lower Z_T: pulse 95962 (Z_T=3-1j Ω) shows better load-resilience (less amplifier trips due to ELMs) than pulse 95957 (Z_T=6-2j Ω). From top to bottom: coupled power (MW), $Re(Z_T)$, VSWR in the Main Transmission Line and Be line intensity representing the ELM activity.

Extensive simulations confirmed the stability of these control mechanisms, accounting for the time constants inherent in various feedback loops [51]. However, complications in implementing poloidal phase control initially restricted the ILA to half-array operation. Full-array operation was later achieved and routinely employed at 33, 37, and 42 MHz, reaching power levels of up to 4.2 MW in H-mode. A poloidal phase scan was performed at 37 MHz [52].

Some control instabilities (capacitors drifting away) were however occasionally observed during full array operation. A possible cause is that the first stage matching

is realised independently, without considering the mutual coupling between the different RDLs. To mitigate these issues, polychromatic operation was tested, whereby the upper and lower halves of the ILA were powered at slightly different frequencies ($f_0 \pm 250$ kHz) [52]. This technique successfully decoupled the control system, eliminating the instability issues. The contribution to the capacitor voltage at the secondary frequency (due to mutual coupling between the two halves of the ILA) was however of the same order of magnitude as the one at the main operating frequency, thereby doubling the capacitor voltage and effectively limiting the achievable power levels compared to monochromatic full-array operation.

3.3.2 Capacitor failures

Despite its innovations, the ILA design had an inherent weakness due to the presence of adjustable in-vessel vacuum capacitors – moving components that required cooling. Over time, wear and tear affected performance, leading to capacitor failures. In 2009, a micro-leak formed in the bellows of one capacitor, halting ILA operation [46]. After refurbishment in 2013, the system was reinstated [54, 55] and continued operating until the early phase of the second Deuterium-Tritium Experimental campaign (DTE2), when another capacitor failed [56, 57]. Temporary measures allowed continued operation between DTE2 and DTE3, but a third capacitor failure ultimately prevented the ILA from contributing to the DTE3 campaign. The ILA nevertheless provided valuable insights into high-power-density operation, complex array control, and SMAD development (see Section 5.1.4).

Following the second capacitor failure, the system was drained; however, residual water remained inside the damaged capacitor and eventually leaked into the torus, forcing a three-week suspension of DTE2 operations. Fortunately, the cooling system's design allowed engineers to pinpoint the source of the leak and safely isolate it. These challenges ultimately validated ITER's decision to avoid adjustable components within the vacuum vessel for its antenna design.

4 Impact of the JET ILW metal wall on the ICRF operation

In 2009, JET operations were paused for two years to replace the original carbon wall (JET-C) with a metal wall (JET-ILW), consisting of a beryllium (Be) first wall and a tungsten (W) divertor [58, 59]. This transition significantly altered plasma recycling and the conditions in the far scrape-off layer. Additionally, during JET-ILW operations, the average plasma-antenna distance was generally larger than during JET-C operation. Consequently, the coupling conditions in JET-ILW were increasingly difficult: the coupling resistance was reduced compared to operation in JET-C and the ELMs were stronger, i.e. exhibited on average larger load variations.

The reduced coupling in JET-ILW necessitated operation at higher maximum voltage. Fortunately, voltage stand-off and conditioning were observed to improve in JET-ILW compared to JET-C. This is illustrated in Fig. 8 where the number of trips recorded during L-mode operation and vacuum conditioning in JET-C and JET-W are compared in function of the maximum applied voltage for the A2 antennas. The improved voltage stand-off in JET-ILW is tentatively attributed, at least in part, to the reduction of carbon dust levels.

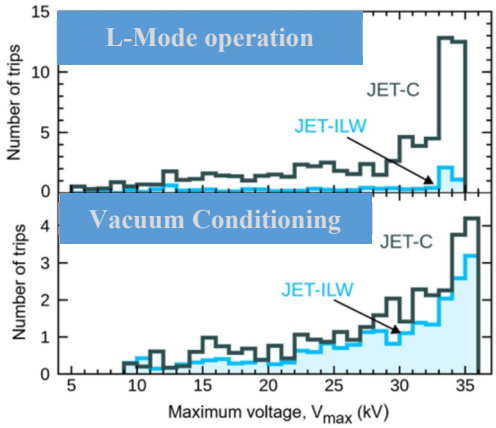

Fig. 8. Comparison of the number of VSWR trips on the JET A2 antenna straps in JET-C and JET-ILW during (top) L-mode operation and (bottom) antenna vacuum conditioning [32].

Despite the more stringent coupling conditions, the A2 antennas generally delivered higher coupled power in JET-ILW than in JET-C, across all operating frequencies. This achievement resulted from a combination of more favourable high-voltage operation conditions and a dedicated effort by the RF team towards better system maintenance, amplifier diagnostics and power optimisation (see Section 5.4).

An extensive overview of JET ICRF operations since 2000, in JET-C and JET-ILW, can be found in [32].

5 Some operation challenges

5.1 Arc detection

5.1.1 The VSWR arc detection

The primary arc detection method in JET relies on the VSWR, derived from directional coupler measurements of the forward and reflected wave amplitudes in the transmission lines [37]. A significant increase in VSWR suggests arcing, triggering a rapid RF power trip (typically within 10–20 µs) to avoid damaging components, and a brief recovery period. ELMs however also result in quickly varying load conditions triggering an increase of VSWR and the power is consequently tripped when the VSWR trip threshold is exceeded. In case of load resilient systems, there is a balance between the protection of the antenna (tripping on arcs) and the load-resilient operation (not tripping on ELMs). Different techniques were developed and implemented to detect arcs in the implemented load-resilient systems.

5.1.2 Arc detection for the 3 dB coupler system

For the 3 dB hybrid coupler system, two VSWR systems operate simultaneously [35, 37]. A 2.4:1 VSWR threshold is set in the Output Transmission Lines (OTLs) – the sections of line between the amplifier and the 3 dB hybrid

splitter. In contrast, an adjustable VSWR protection threshold (3:1, 5:1, 10:1, or 15:1) is applied to the Splitter Transmission Lines (STLs) – the section of lines between the 3 dB hybrid splitter and the antenna straps – allowing higher VSWR ratios to accommodate ELM-induced reflections, while minimizing unnecessary power trips. During ELMs, the 3 dB hybrid splitter redirects the reflected power into a dummy load, isolating amplifiers from load variations and permitting continuous operation.

Arcs formed at low-voltage nodes present another challenge: they do not generate large VSWR increases and can remain undetected, particularly when high VSWR set ratios are used. In some cases, these arcs persist without tripping the amplifier, posing operational risks. One such incident was reported in [60], where a sustained low-voltage arc damaged a VTL bellow. This prompted to carefully monitor the operation with VTL bellows at a voltage node using fast data acquisition of the RF signals.

5.1.3 Arc detection for the ECT system: AWACS

A novel arc detection technique was implemented, in addition to the VSWR system, to enhance arc protection for the ECT: the Advanced Wave Amplitude Comparison System (AWACS) [37, 38]. The AWACS monitors the ratios between the reflected power in the OTL to the forward power in the two branches, CTL and DTL, between the T-junction and the straps of antennas C and D. When an arc forms, the parallel impedance of the line seen at the T-junction increases, reducing current in the affected branch. This results in increased OTL reflected voltage and decreased forward voltage in the affected branch, CTL or DTL. The AWACS is highly sensitive to impedance fluctuations, effectively detecting arcs in CTL and DTL while remaining ELM-tolerant, thus preventing unnecessary power trips.

5.1.4 Arc detection for the ILA system

For the ILA, two advanced arc detection systems were implemented: the innovative S-Matrix Arc Detection (SMAD) and the Sub-Harmonic Arc Detection (SHAD).

The SMAD has been specifically developed to protect the low-voltage area around the T-junction [61-63]. As shown in Fig. 7 operation at low $Re(Z_T)$, hence low voltage at the T-junction, is favourable as it leads to improved load resilience. SMAD performs a consistency check using complex RF measurements around the region of interest (in this case the voltage probe signals on one side and the APTL directional couplers signals on the other side) and an accurate RF model of the region of interest, in this case including the variable vacuum capacitors. A SMAD error is estimated every 2 μs. If this error exceeds a threshold the consistency check fails, triggering a protective trip. Accurate modelling and calibrations [50, 64] are essential for SMAD to be effective.

The SHAD identifies arcs by detecting characteristic sub-harmonic frequencies generated when arcs form. While in principle effective in detecting all arcs, it suffers from false positives due to parasitic signals, such as ion cyclotron emission, fast particle modes or breakdown in the accelerator of the positive ion neutral beam injectors [65]. This limits reliability, and further development of the system was discontinued on JET.

5.2 ICWC and RF-assisted start-up

A dedicated operational scheme was developed to perform Ion Cyclotron Wall Conditioning (ICWC) and RF-assisted plasma start-up experiments. This configuration enables antenna operation in vacuum and in the presence of magnetic field, initiating gas breakdown through radio-frequency (RF) field excitation [56]. These experiments typically use monopole phasing and ensuring RF power is applied prior to gas injection to prevent arcing inside the antenna box. Moreover, operations were conducted below 33 MHz to avoid VTL voltage nodes, which can lead to multipactor-induced discharge.

Due to the sensitivity of vacuum matching, establishing reliable reference pulses before proceeding is essential. Additional protection measures include restricting VSWR settings to 3:1, limiting allowed trips per pulse to 10 (instead of 100), reducing VTL trip soft limits to $5x10^{-5}$ mbar (instead of $1x10^{-4}$ mbar), and setting local MTL voltage limits to 20 kV (instead of 30 kV).

5.3 Deuterium-Tritium operation

Deuterium-Tritium (D-T) operation needed to be planned from start and had a major impact on the design, namely by the requirements of remote handling, material specifications, double vacuum window for tritium containment, etc.

Before D-T operation, additional containment measures were enforced [56, 57]: air flow bleeding of all transmission lines through the Active Handling Gas System (AGHS), extensive survey to reduce the 3-bar pressurised transmission line air leaks, monitoring of the DCF interspace, checking all isolation valves, etc.

Due to the limited neutron and activation budget, the pulses in the DTE2 and DTE3 JET campaigns were considered as a scarce resource. The target was to deliver the full power on the first pulse. It was hence paramount to improve the system reliability and availability by proactive maintenance of the plant and appropriate diagnostic to identify any issue (see Section 5.4). Restricted access to RF buildings further reinforced the necessity of remote monitoring and repairability of the plant.

To optimize performance, amplifiers were systematically tested on test load at the start of each D-T experimental day and after frequency changes. Antenna conditioning minimized arcing risks when operating at high voltages, and reference pulses from prior deuterium campaigns were established under comparable conditions.

5.4 Maximisation of the coupled power

Fig. 9 displays the maximum expected power from all A2 antennas in conditions typical of ELMy H-mode plasmas. Because of the low coupling, the system is generally limited by the maximum allowed voltage in the system, typically set to 30 kV.

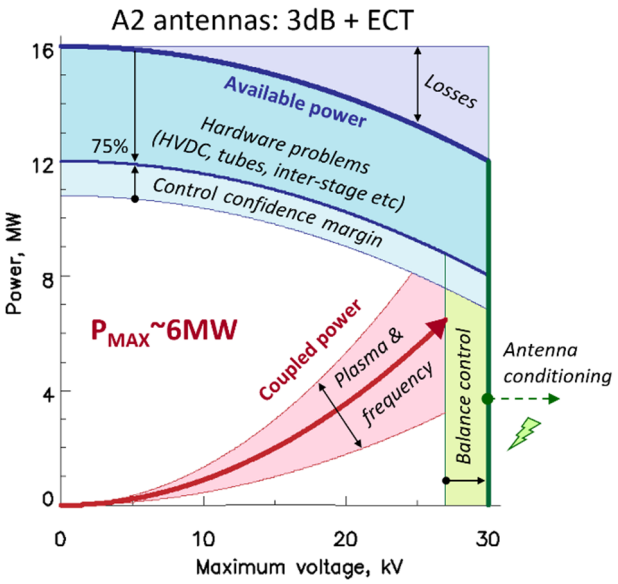

Fig. 9. Expected power from the A2 antennas in load-tolerant configuration (3 dB hybrids + ECT) for typical ELMy H-mode conditions as a function of the maximum voltage in the system.

In case of very good coupling, the power will however be limited by the available power from the amplifier and by the losses in the system. Enhancing power delivery in these conditions (i.e. going upwards in the graph) requires increasing the available power by maintenance of the RF plant and amplifier optimization.

In most cases, the operation is limited by the maximum allowed voltage in the system for given plasma, and hence coupling, conditions. To increase the coupled power, one must allow operating at larger maximum voltage (i.e. going toward the right of the graph). A first option is to optimize the balance control, i.e. tune the system to reach the maximum allowable voltage across all lines. In case of JET, the RF Local Manager (RFLM) was upgraded before DTE2 to equalize voltages taking the plant limits into account [56, 57]. A second option, which requires dedicated time from the operator, is to condition the system for operation at larger voltage.

Finally, the last option is to increase the coupling by acting on the plasma conditions, provided it is compatible with the physics programme. This requires essentially to move the position of the fast wave cut-off density for the considered phasing closer to the antenna. The most efficient ways of improving the coupling are: reducing the plasma-antenna distance, optimizing gas puffing by using gas injection valves close, or at least magnetically connected, to the antenna [66] and increasing of the edge safety factor [32].

Fig. 10 illustrates the benefits of ICRF system conditioning by comparing the two best discharges in DTE2 and DTE3 at same neutral beam power [6]. In the DTE2 pulse, the maximum voltage limit was set to 33 kV, already larger than the usual 30 kV. In DTE3, the system was further conditioned up to 37 kV the day before the experiment and the maximum voltage was set to 35 kV during the experiment. This resulted in an additional ~1.5 MW of RF power, improving impurity screening and discharge stationarity.

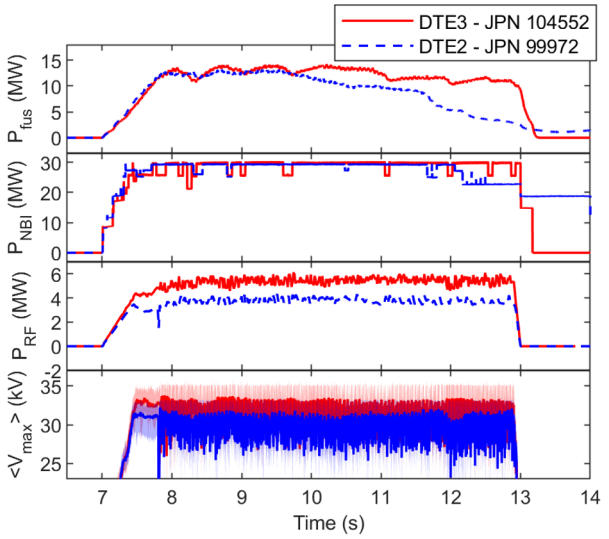

Fig. 10. Comparison of the best performing discharges in DTE2 and DTE3: further conditioning of the ICRF system allowed to operate at larger maximum voltage and improve the stationarity. From top to bottom: fusion power (MW), neutral beam power, ICRF power, maximum voltage on the lines.

6 Lessons learned

The long-term success of JET's ICRF operation was driven by strong early engineering work and sound design decisions. A key approach was to develop a highly flexible and versatile system, ensuring adaptability to evolving physics requirements. Importantly, Deuterium-Tritium (D-T) operation was integrated from the outset, with considerations for material selection, remote handling, and activation management. Every antenna and component underwent rigorous testing before installation to meet current and voltage specifications, while efforts to minimize RF-induced impurity release influenced subsequent design optimizations.

Developing and simulating control tools, including cross-talk modelling and arc detection systems, proved invaluable. The capacitor failures in the ILA highlighted not only the advantage in terms of reliability of avoiding the use of adjustable components inside the vacuum vessel, but also the necessity of rapid fault identification and safe isolation procedures. More broadly, ensuring good accessibility of equipment for efficient maintenance and repair is essential for long-term operational reliability.

It is also important to maintain a power margin: the daily available power often does not match the nominal installed power due to system limitations and faults.

From an operational standpoint, accurate RF measurements and extensive calibration of RF measurements significantly enhance system control and protection. Establishing a robust maintenance and testing schedule for amplifiers, power supplies, and transmission lines is equally critical. On JET, the high-voltage power supplies were generally unavailable during shutdowns, limiting opportunities for amplifier testing and optimization during these periods.

Conditioning remains vital to achieving high maximum voltage operation and reliably delivering increased power output.

Finally, coupling is the most influential factor in system performance and must be optimized through design improvements and active plasma parameter adjustments, such as reducing plasma-antenna distance and optimizing gas injection techniques.

7 Conclusions

The JET project was an extremely ambitious endeavour, marking a significant leap forward in fusion research with its unprecedented scale, power, and physics goals, including the challenging D-T operation. Its success was built on the extraordinary vision and rigorous initial design work, combined with decades of collaborative effort by scientists and engineers from diverse disciplines, united by the shared objective of advancing fusion energy research.

Over its four decades of operation, the JET ICRF system played a crucial role in plasma heating experiments, evolving through multiple generations of antenna designs, operational improvements, and adaptations to new challenges. The project was founded on solid engineering principles, with flexibility and modularity at its core, enabling extraordinary progress in various fields of magnetic confinement fusion research. From the initial prototype A0 antennas to the high performance A1 antennas, the long-lived A2 antennas – 28 years of successful operation – and the later high-power-density ILA system, significant design refinements were made to improve coupling efficiency, impurity control, and load resilience. The challenges represented by the installation of the pumped divertor and the concomitant H-mode operation, the transition from JET-C to JET-ILW and D-T operation were successfully met and several innovative techniques were developed for optimized control and arc protection. Coupling remains the most critical factor in optimizing ICRF system performance.

Ultimately, JET's ICRF system demonstrated remarkable adaptability, achieving record power levels and contributing invaluable insights to fusion research. Contributions to the progress in RF physics understanding and achievements at JET are further detailed in [67] and in a complementary paper by M. Mantsinen et al. [68].

Disclaimer

This work has been carried out within the framework of the EUROfusion Consortium, funded by the European Union via the Euratom Research and Training Programme (Grant Agreement No. 101052200—EUROfusion). Views and opinions expressed are however those of the author(s) only and do not necessarily reflect those of the European Union or the European Commission. Neither the European Union nor the European Commission can be held responsible for them.

References

1. L. A. Artsimovich, S. V. Mirnov, V. S. Strelkov, Investigation of the ohmic heating of a plasma in the 'tokamak-3' toroidal apparatus, J. Nucl. Energy, Part C Plasma Phys. **7**, 305 (1965), https://doi.org/10.1088/0368-3281/7/3/310
2. European Commission, The JET project: design proposal of the joint European Torus, EUR 5516e (EUR-JET-R5), Commission of the European Communities (1976).
3. P. H. Rebut, R. J. Bickerton, B. E. Keen, The Joint European Torus: installation, first results and prospects, Nuclear Fusion, **25**, 1011 (1985). https://doi.org/10.1088/0029-5515/25/9/003
4. P. H. Rebut, B. E. Keen, The JET Experiment: Evolution, Present Status, and Prospects, Fusion Technology **11**, 13 (1987). https://doi.org/10.13182/FST87-A24999
5. F. G. Rimini et al., JET: 40 Successful Years of Fusion Research, IEEE Transactions on Plasma Science **52**, 3561 (2024). https://doi.org/10.1109/TPS.2024.3352233
6. F. G. Rimini et al., 40 years of JET operations: a unique contribution to fusion science, Plasma Phys. Control. Fusion **67**, 033001 (2025), https://doi.org/10.1088/1361-6587/adaee5
7. J. Adam, J. Jacquinot, H. Kuus, Physics aspects and technical elements of an ICRF heating system for JET, EUR-CEA-FC-1065 (1980).
8. T. Wade, R. Anderson, G. Bosia, M. Schmid, JET ICRF power plant, in Fusion Technology 1984,13th Symposium on Fusion Technology, conference centre of Villa Ponti, Varese, Italy, 24-28 September (1984).
9. Equipe TFR, ICRF heating and antenna coupling studies in TFR, Symposium on heating in toroidal plasmas I, Grenoble (France), 22-26 Mar 1982, p. 225-241, Pergamon Press (1982).
10. K. H. Knobbe, H. Noeldge, Long pulse high power ion cyclotron resonance heating generator for TEXTOR, 12th Symposium on Fusion Technology, Jülich, September 13-17 (1982).
11. T. J. Wade, J. Jacquinot, G. Bosia, A. Sibley, M. Schmid, Development of the JET ICRH plant, Fusion Engineering and Design **24**, 23 (1994). https://doi.org/10.1016/0920-3796(94)90035-3
12. P.P. Lallia, P.H. Rebut, Preliminary studies on the JET RF heating system, Symposium on heating in toroidal plasmas III, Grenoble (France), 22-26 Mar 1982, Pergamon Press, 799–811 (1982).

13. J. Jacquinot, R. Anderson, J. Arbez, D. Bartlett, B. Beaumont, et al., Preliminary ICRF results from JET, Plasma Physics and Controlled Fusion **27**, 1379 (1985). https://doi.org/10.1088/0741-3335/27/12A/005

14. T.J. Wade, G. Bosia, M. Schmid, A. Sibley, Automatic ICRH power coupling to any plasma in JET, 12th Symposium on Fusion Engineering, Monterey, CA (USA)., 12-16 Oct 1987, 1200 (1987).

15. V. P. Bhatnagar, G. Bosia, P Dhondt, R. Koch, A. Messiaen, et al., ICRH in the Erasmus tokamak at power levels exceeding that of ohmic heating, 8th International Conference on Plasma Physics and Controlled Nuclear Fusion Research, Brussels, **2**, 85, IAEA-CN-38/D-4 (1980).

16. J. Hosea, D. Boyd, N. Bretz, R. Chrien, S. Cohen, et al., Fast-wave ion cyclotron heating in the Princeton Large Torus, 8th International Conference on Plasma Physics and Controlled Nuclear Fusion Research, Brussels, **2**, 85, IAEA-CN-38/D-5-1 (1980).

17. J. Arbez, B. Beaumont, E. Hanley, J. Jacquinot, A. Kaye et al., The JET ICRF Antenna System, Int. Symp. on Heating in Toroidal Plasmas, Rome, 1244 (1984).

18. J. Arbez, B. Beaumont, A. Franklin, E. Hanley, J. Jacquinot, A. Kaye, et al., The JET ICRF antennae systems: Description and test bed results, 13th Symposium on Fusion Technology, Varese (Italy), 24-28 Sep 1984, Pergamon Press, 669 (1985)

19. A. Kaye, J. Jacquinot, P. Lallia, T. Wade, Radio-frequency heating system, Fusion Technology **11**, 203 (1987). https://doi.org/10.13182/FST11-203-234

20. J. Jacquinot, V. Bhatnagar, H. Brinkschulte, M. Bures, S. Corti, et al., Additional heating experiments on JET with ion-cyclotron waves, Philos. Trans. R. Soc. London, Ser. A, **322**, 95 (1987). https://doi.org/10.1098/rsta.1987.0040

21. J. Jacquinot, et al., High power ion cyclotron resonance heating in JET. Plasma Physics and Controlled Fusion **30**, 1467 (1988). https://doi.org/10.1088/0741-3335/30/11/009

22. J. Jacquinot, M. Keilhacker, P. H. Rebut, Chapter 2: Mission and highlights of the JET joint undertaking: 1978-1999. Fusion Science and Technology, **53**, 866 (2008). https://doi.org/10.13182/FST08-A1742

23. J. Jacquinot, V. P. Bhatnagar, A. Kaye, T. Brown, Launching fast waves in large devices, IAEA technical committee meeting on RF launchers for plasma heating and current drive, Naka, Ibaraki (Japan), 10-12 Nov 1993, JAERI-Conf--94-001, 3–14 (1994)

24. A. Kaye, T. Brown, V. Bhatnagar, P. Crawley, J. Jacquinot, R. Lobel, et al., Present and future JET ICRF antennae, Fusion Engineering and Design, **24(1-2)**, 1-21 (1994), https://doi.org/10.1016/0920-3796(94)90034-5

25. G. Bosia, B. Lamont, 1. Sibley, M. Schmid, T. Wade, Automatic VSWR control in JET ICRH transmitters, Fusion Technology, 16th Symp., London, 3-7 September 1990, Amsterdam, North Holland, **2**, 1099 (1991).

26. A. Sibley, V. Bhatnagar, G. Bosia, M. Bures, J. A. Dobbing, et al., Power optimisation in the RF systems at JET and future devices, 15th IEEE/NPSS Symposium on Fusion Engineering-Supplement, IEEE, 62 (1993). https://doi.org/10.1109/SFE.1993.472783

27. C.I. Walker, H. Brinkschulte, M. Bures, N. Dragomelo, J.P. Coad, et al., The JET ICRF Antennae screen: experience with the actively cooled nickel screen and design of a new beryllium screen, 15th SOFT, Utrecht, 1988, Elsevier Science Publishers **1**, 444 (1989).

28. M. Bures, J. J. Jacquinot, M. F. Stamp, D. D. R. Summers, D. F. H., Start, et al., Assessment of beryllium Faraday screens on the JET ICRF antennas. Nuclear fusion, **32(7)**, 1139 (1992). https://doi.org/10.1088/0029-5515/32/7/I05

29. V.P. Bhatnagar, J. Jacquinot, C. Gormezano, D.F.H. Start, ICRF Heating and Synergistic LH and Fast-Wave Current Drive in JET, AIP Conf. Proc. **244**, 115 (1992). https://doi.org/10.1063/1.41700

30. A. Messiaen, R. Weynants, ICRH antenna coupling physics and optimum plasma edge density profile. Application to ITER, Plasma Phys. Control. Fusion **53**, 085020 (2011). https://doi.org/10.1088/0741-3335/53/8/085020

31. E. Lerche, D. Van Eester, J. Ongena, M.-L. Mayoral, M. Laxaback, et al., Optimizing ion-cyclotron resonance frequency heating for ITER: dedicated JET experiments, Plasma Phys. Control. Fusion **53**, 124019 (2011). https://doi.org/10.1088/0741-3335/53/12/124019

32. I. Monakhov, P. Jacquet, P. Dumortier, F. Durodié, E. Lerche, et al., Assessment of the JET ICRH system performance since 2000, Plasma Phys. Control. Fusion **67**, 015023 (2025). https://doi.org/10.1088/1361-6587/ad9e73

33. A.S. Kaye, V. Bhatnagar, M. Bures, P. Crawley, B. Fechner, et al., ICRF system in the JET pumped divertor configuration, 16th International Symposium on Fusion Engineering, Champaign, IL, USA, **1**, 736-741 (1995). https://doi.org/10.1109/FUSION.1995.534328

34. F. Wagner, G. Becker, K. Behringer, D. Campbell, A. Eberhagen et al., Regime of Improved Confinement and High Beta in Neutral-Beam-Heated Divertor Discharges of the ASDEX Tokamak, Phys. Rev. Lett. **49**, 1408 (1982). https://doi.org/10.1103/PhysRevLett.49.1408

35. M. Mayoral, I. Monakhov, T. Walden, V. Bobkov, T. Blackman, et al., Hybrid couplers on the JET ICRF system: commissioning and first results on ELMs, in AIP Conf. Proc. **933**, 143–146 (2007), https://doi.org/10.1063/1.2800462

36. M. Nightingale, F. Durodie, A. Argouarch, G. Berger-By, T. Blackman, et al., Development of the JET ion cyclotron resonance frequency heating system in support of ITER, 22nd IAEA Fusion Energy Conference, International Atomic Energy Agency, **103** (2008).

37. M. Graham, M. L. Mayoral, I. Monakhov, J. Ongena, T. Blackman, et al., Implementation of load resilient ion cyclotron resonant frequency (ICRF) systems to couple high levels of ICRF power to ELMy H-mode plasmas in JET, Plasma Physics and Controlled Fusion **54**, 074011 (2012). https://doi.org/10.1088/0741-3335/54/7/074011

38. I. Monakhov, M. Graham, T. Blackman, S. Dowson, F. Durodie, et al., Design and operations of a load-tolerant external conjugate-T matching system for the A2 ICRH antennas at JET, Nuclear Fusion **53**, 083013 (2013). https://doi.org/10.1088/0029-5515/53/8/083013

39. P. U. Lamalle, R. Goulding, I. Monakhov, A. G. H. Sibley, M. Simon, et al., Commissioning of the wideband matching system for ICRH of ELMy JET plasmas, in AIP Conf. Proc. **595**, 118 (2001). https://doi.org/10.1063/1.1424158

40. F. Durodié, P. Lamalle, G. Agarici, G. Amarante, W. Baity, et al., JET-EP ITER-like ICRF antenna, AIP Conf. Proc. **595**, 122 (2001). https://doi.org/10.1063/1.1424159

41. F. Durodié, G. Agarici, G. Amarante, F. W. Baity, B. Beaumont, et al., The ITER-like ICRH Launcher Project For JET, AIP Conf. Proc. **694**, 98 (2003). https://doi.org/10.1063/1.1638003

42. F. Durodié, Ph. Chappuis, J. Fanthome, R.H. Goulding, J. Hosea, et al., Main design features and challenges of the ITER-like ICRF antenna for JET, Fus. Eng. Des. **74**, 223 (2005). https://doi.org/10.1016/j.fusengdes.2005.08.019

43. F. Durodié, M. Nightingale, A. Argouarch, G. Berger-By, T. Blackman, et al., Commissioning of the ITER-like ICRF antenna for JET, Fus. Eng. Des. **84**, 279 (2009). https://doi.org/10.1016/j.fusengdes.2009.01.074

44. F. Durodié, M. Nightingale, M.-L. Mayoral, A. Argouarch, T. Blackman, et al., Present Status of the ITER-like ICRF Antenna on JET, AIP Conf. Proc. **1187**, 221–224 (2009). https://doi.org/10.1063/1.3273733

45. M.P.S. Nightingale, F. Durodie, A. Argouarch, B. Beaumont, A. Becoulet, et al., Overview on experiments on ITER-like antenna on JET And ICRF antenna design for ITER, AIP Conf. Proc. **1187**, 213–220 (2009). https://doi.org/10.1063/1.3273731

46. F. Durodié, M.P.S. Nightingale, M.-L. Mayoral, J. Ongena, A. Argouarch, et al., Physics and engineering results obtained with the ion cyclotron range of frequencies ITER-like antenna on JET, Plasma Phys. Control. Fusion **54**, 074012 (2012). https://doi.org/10.1088/0741-3335/54/7/074012

47. A. Czarnecka, F. Durodié, A.C.A. Figueiredo, K.D. Lawson, E. Lerche, et al., Impurity production from the ion cyclotron resonance heating antennas in JET, Plasma Phys. Control. Fusion **54**, 074013 (2012). https://doi.org/10.1088/0741-3335/54/7/074013

48. V. Bobkov, D. Aguiam, M. Baruzzo, D. Borodin, I. Borodkina, et al., Progress in reducing ICRF-specific impurity release in ASDEX upgrade and JET, Nuclear Materials and Energy **12**, 1194 (2017). https://dx.doi.org/10.1016/j.nme.2016.10.026

49. R.H. Goulding, F.W. Baity, K.D. Freudenberg, G.H. Jones, B.E. Nelson, D.A. Rasmussen, et al., Results and implications of the JET ITER-like ICRF antenna high power prototype tests, 20th IAEA fusion energy conference 2004, Villamoura (Portugal), 1-6 Nov 2004 (2005).

50. W. Helou, P. Dumortier, F. Durodié, G. Lombard, K. Nicholls, et al., ITER-like antenna capacitors voltage probes: Circuit/electromagnetic calculations and calibrations, Rev. Sci. Instrum. **87**, 104705 (2016). https://doi.org/10.1063/1.4964137

51. F. Durodié, P. Dumortier, W. Helou, A. Křivská, E. Lerche, et al., Circuit model of the ITER-like antenna for JET and simulation of its control algorithms, AIP Conf. Proc. **1689**, 070013 (2015). https://doi.org/10.1063/1.4936520

52. P. Dumortier, F. Durodié, P. Jacquet, E. Lerche, I. Monakhov, et al., JET ILA full array and polychromatic operation, Fus. Eng. Des. **169**, 112489 (2021). https://doi.org/10.1016/j.fusengdes.2021.112489

53. F. Durodié, P. Dumortier, T. Blackman, E. Wooldridge, E. Lerche, et al., ITER-like antenna for JET first results of the advanced matching control algorithms, Fus. Eng. and Des. **123**, 253 (2017). https://doi.org/10.1016/j.fusengdes.2017.05.113

54. P. Dumortier, F. Durodié, T. Blackman, M. Graham, W. Helou, et al., Commissioning and first results of the reinstated JET ICRF ILA, Fus. Eng. Des. **123**, 285 (2017). https://doi.org/10.1016/j.fusengdes.2017.05.050

55. P. Dumortier, F. Durodié, T. Blackman, W. Helou, P. Jacquet, et al., Reinstated JET ICRF ILA: Overview and Results, EPJ Web of Conferences **157**, 03010 (2017). https://doi.org/10.1051/epjconf/201715703010

56. P. Jacquet, P. Dumortier, E. Lerche, I. Monakhov, C. Noble, et al., ICRH operations during the JET tritium and DTE2 campaigns, Nucl. Fusion **64**, 066039 (2024). https://doi.org/10.1088/1741-4326/ad3f2c

57. P. Jacquet; E. Lerche; M. Mantsinen; D. Van Eester; K. Kirov, et al., ICRH operations and experiments during the JET-ILW tritium and DTE2 campaigns, AIP Conf. Proc. **2984**, 030003 (2023). https://doi.org/10.1063/5.0162645

58. J. Paméla, G. F. Matthews, V. Philipps, R. Kamendje, An ITER-like wall for JET, J. Nucl. Mater. **363**, 1 (2007). https://doi.org/10.1016/j.jnucmat.2006.12.056

59. M.-L. Mayoral, V. Bobkov, A. Czarnecka, I. Day, A. Ekedahl, et al., On the challenge of plasma heating with the JET metallic wall, Nucl. Fusion **54**, 033002 (2014). https://doi.org/10.1088/0029-5515/54/3/033002

60. I. Monakhov, V. Bobkov, M. Graham, M. L. Mayoral, K. Nicholls, et al., Voltage node arcing in the ICRH antenna vacuum transmission lines at JET, AIP Conf. Proc. **933**, 151 (2007). https://doi.org/10.1063/1.2800464

61. M. Vrancken, A. Argouarch, T. Blackman, P. Dumortier, F. Durodié, et al., Scattering-matrix arc detection on the JET ITER-like ICRH antenna, Fus. Eng. Des. **84**, 1953 (2009), https://doi.org/10.1016/j.fusengdes.2008.11.035

62. M. Vrancken, E. Lerche, T. Blackman, F. Durodié, M. Evrard, et al., Performance of the Scattering Matrix Arc Detection System on the JET ITER-like ICRF antenna, Fus. Eng. and Des. **86**, 522 (2011). https://doi.org/10.1016/j.fusengdes.2011.02.056

63. P. Dumortier, E. Lerche, F. Durodié, T. Blackman, W. Helou, et al., Review of the JET ILA scattering-matrix arc detection system, Fus. Eng. Des. **150**, 110669 (2020). https://doi.org/10.1016/j.fusengdes.2019.01.085

64. P. Dumortier, F. Durodié, W. Helou, I. Monakhov, C. Noble, et al., Calibrations and verifications performed in view of the ILA reinstatement at JET, AIP Conf. Proc. **1689**, 070003 (2015). https://doi.org/10.1063/1.4936510

65. P. Jacquet, G. Berger-By, V. Bobkov, T. Blackman, I.E. Day, et al., Parasitic signals in the receiving band of the Sub-Harmonic Arc Detection system on JET ICRF Antennas, AIP Conf. Proc. **1406**,17–20 (2011). https://doi.org/10.1063/1.3664919

66. P. Jacquet, M. Goniche, V. Bobkov, E. Lerche, R.I. Pinsker, et al., Maximization of ICRF power by SOL density tailoring with local gas injection, Nucl. Fusion **56**, 046001 (2016). https://doi.org/10.1088/0029-5515/56/4/046001

67. J.-M. Noterdaeme, L.-G. Eriksson, M. Mantsinen, M.-L. Mayoral, D. Van Eester, et al., Chapter 9: Physics studies with the additional heating in JET, Fusion Science and Technology **53,** 1103 (2008). https://doi.org/10.13182/FST08-A1749

68. M. J. Mantsinen et al., 40 Years of ICRF Physics on the JET Tokamak: Highlights and Lessons Learned for Future Facilities, 25th Topical Conference on Radio-Frequency Power in Plasmas, Schloss Hohenkammer, Germany, May 19-22 (2025). https://www.ipp.mpg.de/5533680